Using K_{DP} Cores as a Downburst Precursor Signature

CHARLES M. KUSTER,[a,b,c] BARRY R. BOWERS,[d] JACOB T. CARLIN,[a,b,c] TERRY J. SCHUUR,[a,b,c]
JEFF W. BROGDEN,[a,b,c] ROBERT TOOMEY,[a,b,c] AND ANDY DEAN[e]

[a] *Cooperative Institute for Mesoscale Meteorological Studies, Norman, Oklahoma*
[b] *NOAA/OAR/National Severe Storms Laboratory, Norman, Oklahoma*
[c] *University of Oklahoma, Norman, Oklahoma*
[d] *NOAA/National Weather Service, Norman, Oklahoma*
[e] *NOAA/NWS/NCEP Storm Prediction Center, Norman, Oklahoma*

(Manuscript received 7 January 2021, in final form 19 April 2021)

ABSTRACT: Decades of research have investigated processes that contribute to downburst development, as well as identified precursor radar signatures that can accompany these events. These advancements have increased downburst predictability, but downbursts still pose a significant forecast challenge, especially in low-shear environments that produce short-lived single and multicell thunderstorms. Additional information provided by dual-polarization radar data may prove useful in anticipating downburst development. One such radar signature is the K_{DP} core (where K_{DP} is the specific differential phase), which can indicate processes such as melting and precipitation loading that increase negative buoyancy and can result in downburst development. Therefore, K_{DP} cores associated with 81 different downbursts across 10 states are examined to explore if this signature could provide forecasters with a reliable and useable downburst precursor signature. The K_{DP} core characteristics near the environmental melting layer, vertical gradients of K_{DP}, and environmental conditions were quantified to identify any differences between downbursts of varying intensities. The analysis shows that 1) K_{DP} cores near the environmental melting layer are a reliable signal that a downburst will develop; 2) while using K_{DP} cores to anticipate an impending downburst's intensity is challenging, larger K_{DP} near the melting layer and larger vertical gradients of K_{DP} are more commonly associated with strong downbursts than weak ones; 3) downbursts occurring in environments with less favorable conditions for downbursts are associated with higher magnitude K_{DP} cores, and 4) K_{DP} cores evolve relatively slowly (typically longer than 15 min), which makes them easily observable with the 5-min volumetric updates currently provided by operational radars.

KEYWORDS: Downbursts; Storm environments; Thunderstorms; Radars/Radar observations; Nowcasting

1. Introduction

Downbursts, defined as localized areas of strong, often damaging winds caused by especially strong downdrafts in convective storms, pose a significant challenge to National Weather Service (NWS) forecasters (e.g., Fujita and Byers 1977; Fujita and Wakimoto 1981). Over the years, researchers have discovered several radar signatures that provide clues about downbursts before they develop. These precursor signatures include descending reflectivity cores (e.g., Isaminger 1988; Roberts and Wilson 1989), midlevel radial convergence (e.g., Roberts and Wilson 1989; Straka and Anderson 1993), and differential reflectivity (Z_{DR}) holes, troughs, and columns (e.g., Bringi et al. 1984; Wakimoto and Bringi 1988; Scharfenberg 2003; Ryzhkov et al. 2013; Amiot et al. 2019). The potential benefit of these signatures to warn on downbursts is demonstrated by Isaminger (1988), who showed that 95% of downbursts in a specialized study near Huntsville, Alabama, were preceded by a descending reflectivity core, and Ryzhkov et al. (2013), who found that vertical depth of a Z_{DR} hole was related to downdraft velocity.

Despite increased knowledge about downburst precursor signatures and their role in anticipating downburst development, predicting downbursts remains challenging, especially for low-shear environments with single-cell and multicell thunderstorms (e.g., Smith et al. 2004; Miller and Mote 2018). One potential reason for this challenge is that downbursts and their precursor signatures are small-scale events that evolve quickly and can be difficult to detect using available tools such as weather radar (e.g., Fujita 1981; Heinselman et al. 2008; LaDue et al. 2010). For example, using rapid-update data from a research phased array radar (e.g., Forsyth et al. 2005; Zrnić et al. 2007), Heinselman et al. (2008) observed a high-reflectivity core develop and descend in only about 7 min within a downburst-producing storm. With these challenges in mind, it is possible that new radar technology (e.g., phased array radars) or the identification of additional precursor signatures may be needed to increase downburst predictability.

Recently, National Weather Service (NWS) forecasters at the Norman, Oklahoma, Weather Forecast Office and elsewhere (e.g., Frugis 2018) have noticed that an area of enhanced positive specific differential phase (K_{DP}) near and below the environmental melting layer, known as a K_{DP} core (e.g., Jung et al. 2012; Kumjian et al. 2019), appears to be associated with downburst-producing storms. Therefore, the purpose of this

Supplemental information related to this paper is available at the Journals Online website: https://doi.org/10.1175/WAF-D-21-0005.s1.

Corresponding author: Charles M. Kuster, Charles.Kuster@noaa.gov

DOI: 10.1175/WAF-D-21-0005.1

TABLE 1. Number of strong and weak downbursts as well as event dates for each state. Total downburst counts and case dates are included in the bottom row.

State	No. of strong downbursts	No. of weak downbursts	Dates
Alabama	3	2	9 Jun 2018, 11 Jun 2018
Arizona	8	0	27 Aug 2015, 9 Jul 2018
Florida	1	2	21 Jul 2017
Georgia	5	1	17 Jun 2015, 22 Jun 2015, 21 Jul 2017
Kansas	5	1	30 Jul 2013, 25 Jul 2014, 19 Aug 2016
Kentucky	2	0	4 Jul 2018
Ohio	3	0	4 Aug 2018
Oklahoma	12 (4 rapid update, 8 traditional update)	17 (12 rapid update, 5 traditional update)	8 Jul 2014, 29 Jun 2015, 30 Jun 2016, 27 Jul 2016, 27 Jul 2017, 13 Jun 2018, 7 Aug 2018, 17 Aug 2019
South Carolina	2	0	22 Jun 2015, 7 Aug 2016
Tennessee	9	8	15 Jun 2018, 17 Jun 2018
Totals	50 strong downbursts	31 weak downbursts	24 dates

study is to examine K_{DP} core evolution for 81 downbursts of varying intensities across multiple geographic regions to explore what K_{DP} cores might reveal about impending downburst development and intensity (section 2). To determine whether or not K_{DP} cores could be a reliable downburst precursor signature, we examine K_{DP} cores in the context of downdraft conceptual models (section 3), analyze K_{DP} core evolution near the environmental melting layer (section 4), and investigate their vertical gradient below the environmental melting layer (section 5). We also discuss K_{DP} cores in the context of environmental information, present a case study (section 6), and examine the impact of radar update time on observing this downburst precursor signature (section 7).

2. Radar data methods and weather event information

To focus the analysis on downbursts associated with single and multicell storms, we searched for days that contained severe wind reports, isolated storms, and deep-layer shear (i.e., 0–6 km) of about 15.4 m s^{-1} (30 kt) or less. Additionally, to minimize issues associated with beam broadening and poor near-ground data coverage due to relatively high minimum beam height, we only looked at storms within 100 km of the nearest Weather Surveillance Radar-1988 Doppler (WSR-88D). Based on these criteria, we selected 687 radar volume scans from 81 downbursts occurring on 24 unique days for analysis. Though all selected days had severe wind reports ($\geq$50 kt; 25.7 m s^{-1}), not all of the selected downbursts were associated with a severe wind report. All downbursts occurred within 10 states spanning from Florida to Arizona during the months of June, July, and August (Table 1) and were all wet downbursts since they were associated with rain greater than 0.01 in at the surface (e.g., Wakimoto 1985). Of the 24 downburst days, 4 had rapid-update (i.e., volumetric update times of $\leq$2.2 min) data collected by a research WSR-88D located in Norman, Oklahoma (KOUN). Volumetric update times for all other cases ranged from 4.0 to 7.1 min depending on the scanning strategy employed by the NWS during real-time operations. The presence of KOUN as well as the Oklahoma Mesonet, which provides dense near-surface wind observations (e.g., Brock et al. 1995; McPherson et al. 2007), resulted in more cases being selected in Oklahoma than any other state (Table 1). All radar data used were from S-band radars, so the results of this study are only directly applicable to S-band radars since radar wavelength affects estimates of K_{DP} (e.g., Ryzhkov et al. 2013; Augros et al. 2016).

The K_{DP} core ($K_{DP} \geq 1.0°$ km^{-1} near or within 3 km below the environmental melting layer) analysis began when the K_{DP} core developed, which occurred no longer than 31 min (mean of 15 min) prior to downburst development—the time when the velocity difference across a downburst's divergent signature reached 10 m s^{-1} on the lowest-elevation angle (Wilson et al. 1984). Analysis continued until the K_{DP} core dissipated, which occurred after the time of downburst maximum intensity—the time when the maximum radial velocity occurred within each downburst's divergent signature on the lowest-elevation angle—in all but three of the analyzed downbursts. This analysis window ranged from 8.5 to 71.5 min (median of 29.5 min) and should adequately capture the full evolution of the precursor signature (e.g., Isaminger 1988; Wakimoto and Bringi 1988; Amoit et al. 2019). The 1.0° km^{-1} threshold for defining K_{DP} cores was chosen because it was the most effective threshold for separating individual K_{DP} cores in instances of multicell convection, though other thresholds could be tried in future work. All K_{DP} calculations were performed using the method currently used by the NWS (Ryzhkov et al. 2005). It is also important to remember that K_{DP} is not provided in WSR-88D data where reduced correlation coefficient (<0.90) is present, such as in substantial mixed-phase precipitation. We did not encounter many examples of this issue in our dataset, but it is likely to occur at least occasionally in operational settings.

One of the greatest challenges we faced was accurately measuring and classifying the true intensity of each downburst. The National Centers for Environmental Information (NCEI) Storm Events Database has limitations including overestimations of wind speed (e.g., Trapp et al. 2006). Meanwhile, radars only measure the wind's radial component, and that measurement is impacted by a storm's distance from the radar since resolution decreases and minimum beam height increases at greater distances. It is therefore likely that radar undersamples downburst intensity especially for shallow downbursts at larger distances from the radar. Ultimately, we classified individual downbursts as ''strong'' or ''weak'' using a combination of thunderstorm wind reports [i.e., measured gust of $\geq$25.7 m s^{-1} (50 kt) and/or damage] from NCEI and Doppler velocity data. A downburst was classified as ''strong'' if it was associated with a wind report or a maximum 0.5° radial velocity of $\geq$23 m s^{-1}, which represented the 75th percentile of all downbursts' maximum observed radial velocity in this study. Using this method, 15 downbursts were classified as ''strong'' because they were associated with both a wind report *and* maximum radial velocity of $\geq$23 m s^{-1}, 33 were classified as ''strong'' because they were associated with only a wind report, 2 were classified as ''strong'' because they had only a maximum radial velocity of $\geq$23 m s^{-1}, and 31 were classified as ''weak'' because they were not associated with a wind report and had a maximum radial velocity $<$ 23 m s^{-1} (Table 1).

3. K_{DP} cores and scientific conceptual models

Downbursts develop in response to a strong downdraft reaching the surface (e.g., Fujita and Byers 1977; Fujita and Wakimoto 1981). The acceleration of these downdrafts is initiated and strengthened by negative buoyancy due to precipitation loading (e.g., Proctor 1988; Kingsmill and Wakimoto 1990), diabatic cooling processes including the melting of graupel and hail (e.g., Srivastava 1987; Straka and Anderson 1993), and evaporation of raindrops (e.g., Srivastava 1985; Wakimoto 1985), both of which are related to the amount of precipitation in a volume. The ambient environment is also an important control on the relative efficiency of the diabatic cooling processes generating negative buoyancy, which makes environmental information a crucial component of any conceptual model employed by forecasters to anticipate downbursts (e.g., Atkins and Wakimoto 1991; McNulty 1991).

Dual-polarization (dual-pol) radar signatures that provide information about these sources of negative buoyancy are likely to be beneficial to forecasters for downburst detection. Past studies have shown that some Z_{DR} signatures, such as a ''Z_{DR} hole,'' which consists of low values of Z_{DR} located beneath the environmental melting layer that typically increase in magnitude with decreasing height, indicate the presence of melting hail and may provide insight that a downburst could be developing (e.g., Wakimoto and Bringi 1988; Mahale et al. 2016; Amiot et al. 2019). However, both Z and Z_{DR} are most strongly affected by the largest particles that typically comprise only a small fraction of the total precipitation mass. For this reason, Z in mixtures of rain and hail cannot be used to reliably estimate the precipitation content in a radar volume (Carlin et al. 2016), and, while Z_{DR} is useful for identifying large hail (e.g., Heinselman and Ryzhkov 2006), which one can use to infer the presence of a downdraft, its utility for detecting developing downbursts may be more limited than K_{DP}.

Comparatively few studies concerning downburst detection have focused on K_{DP} signatures. The K_{DP} describes the rate that a phase difference accumulates between the horizontal and vertical wave polarizations as they pass through precipitation and, like Z, is more sensitive to liquid water than ice. Since raindrops become increasingly nonspherical (i.e., oblate) with size, the horizontal wave phase shifts more than its vertical counterpart and thus increases K_{DP}, with values increasing more for more oblate and larger numbers of raindrops (i.e., increased liquid mass). Conversely, dry hailstones, which are ice and tend to be more spherical (at least in a bulk sense) than raindrops, are characterized by lower K_{DP}. It is the relative insensitivity to ice of K_{DP} that explains the widespread adoption of K_{DP} for isolating and quantitatively estimating liquid precipitation in the presence of hail (e.g., Seliga and Bringi 1978; Hubbert et al. 1998; Kumjian 2013). The K_{DP} of melting graupel and hail depends on the distribution and shape of the meltwater (e.g., Ryzhkov et al. 2013, Kumjian et al. 2018) and the degree of meltwater shedding (e.g., Rasmussen and Heymsfield 1987), but it generally increases during the melting process from near zero in dry ice toward increasingly positive values in raindrops as the size and number of drops increases.

Given its robust relationship to liquid water content, K_{DP} appears to be useful for identifying regions of ongoing negative buoyancy generation responsible for downbursts. For typical graupel and hail particle size distributions in low-shear environments (e.g., Auer 1972; Field et al. 2019), the majority of mass is concentrated among graupel and smaller hail particles, which begin rapidly melting and quickly increase the K_{DP} near and below the environmental melting layer (e.g., Kumjian et al. 2019). Similarly, because the K_{DP} of dry hail is near 0° km^{-1}, the rate of increase of K_{DP} below the environmental melting level is proportional to the rate of meltwater generation and thus the cooling rate due to melting. Thus, all else being constant, a sudden increase in K_{DP} below the environmental melting level likely indicates a significant amount of precipitation descending, melting, and generating negative buoyancy that may lead to the formation of a downburst. Indeed, evidence is emerging from observations by operational meteorologists that descending K_{DP} cores are associated with downbursts (e.g., Frugis 2018, 2020).

In reality, there are factors that may complicate these idealized conceptual relations. The description above is parcel-centric, which is based on the implicit assumption of the hydrometeor distribution remaining unchanged as a downdraft descends. This assumption neglects changes in the precipitation core owing to size sorting due to differential fall speeds or the mixing of different hydrometeor populations more generally. In addition, the wet growth of hail or rain/hail mixtures within and near convective storm updrafts may result in enhanced K_{DP} above the environmental melting level (e.g., Hubbert et al. 1998; Loney et al. 2002; Snyder et al. 2017). Meltwater behavior on large hailstones and its shedding, along with the breakup of large raindrops from melted ice, can also affect the resultant K_{DP} despite conserving water mass. More importantly, cooling due to evaporation is also a significant source of negative buoyancy but *decreases* K_{DP}. While this relationship is likely a complicating factor in dry environments typically found in the western United States, we believe K_{DP} near the melting level is still a useful metric as many downburst environments (e.g., deep, well-mixed boundary layers) are moist near 0°C and become progressively drier toward the surface so that the majority of ice mass melts quickly with initially limited evaporative losses. In addition, higher K_{DP} maximums below the environmental 0°C level from melting also indicate the potential for more evaporative cooling, even as the sign of the K_{DP} gradient switches.

4. K_{DP} core characteristics at the environmental melting layer

To measure K_{DP} core evolution near the environmental melting layer over time, we calculated the median and maximum values as well as the size (i.e., quasi-horizontal cross-sectional area) for all K_{DP} values ≥ 1.0° km^{-1} within the core at the elevation angle closest to the height of the environmental melting layer. The elevation angle closest to the environmental melting layer occasionally changed as a given downburst-producing storm moved toward or away from the radar. This change in elevation angle—and accompanying change in beam height—sometimes caused an artificial "jump" in K_{DP} core median and maximum value and size, but since these "jumps" were not common, we do not believe they significantly impacted the results presented below. We determined the approximate environmental melting layer height using a combination of the 0°C height from the nearest available observed sounding and Rapid-Refresh model output as well as dual-pol radar data near the storms of interest. The resulting height was typically 100–300 m below the observed/modeled 0°C height and likely close to the wet-bulb 0°C height. These calculations were performed for every volume scan (n = 687) during the K_{DP} core's life cycle (i.e., development to dissipation time; section 2).

a. *K_{DP} cores precede downburst development and intensification*

Our analysis revealed that all 81 downbursts in our study were associated with a K_{DP} core with 75% exhibiting a temporal peak (i.e., local maximum over time) in maximum K_{DP} near the environmental melting layer prior to the downburst's maximum intensity. The remaining 25% were associated with a K_{DP} core but the trends in K_{DP} maximums over time were either decreasing or steady prior to downburst maximum intensity so no local peak was observed. We also looked for K_{DP} cores that were not associated with downbursts (i.e., no 0.5° divergent signature with a velocity difference of ≥10 m s^{-1}) and were only able to identify two such null events within 100 km of a radar across all 24 case days considered. It is therefore possible that the false alarm ratio associated with K_{DP} cores is quite low, at least on days where the environment is supportive of downburst development, though additional study is needed. In favorable environments, it is likely that if a K_{DP} core is observed a downburst of some magnitude will occur.

To examine K_{DP} core evolution relative to downburst evolution, we calculated lag correlations between K_{DP} core maximum value (i.e., maximum value of K_{DP} within the K_{DP} core; hereafter referred to as K_{DP} core maximum) and size near the environmental melting layer and maximum radial velocity at the lowest-elevation angle and then used a bootstrapping method with replacement (n = 5000) to determine statistical significance. Of the 81 total downbursts, 6 downbursts had fewer than 4 volume scans of data (i.e., K_{DP} core dissipated within ~20 min of developing) and were excluded from the lag correlation analysis. Any positive correlation at a negative lag time indicates that increases in K_{DP} core maximum or size precede increases in maximum radial velocity at the lowest-elevation angle. Statistically significant (i.e., 90% confidence level) positive correlations occurred at lags of −3 volume scans for K_{DP} core maximum and from −2 to −3 volume scans for K_{DP} core size (Fig. 1). Assuming an average volume update time of 5 min for these cases (traditional WSR-88D data and degraded—i.e., retained every third volume scan—KOUN data that nearly matched the volumetric update time of the WSR-88D network), a forecaster seeing an increase in K_{DP} core maximum or size could expect to see an increase in downburst intensity in the next 10–20 min and this time scale fits well with the time scales presented in Srivastava (1987).

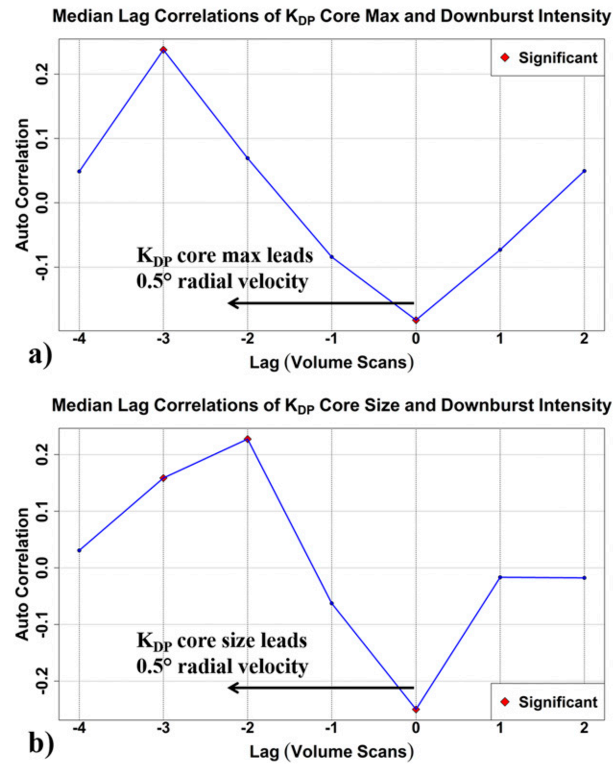

FIG. 1. Median lag correlations between (a) K_{DP} core maximum near the environmental melting layer and 0.5° radial velocity within a downburst's near-surface divergent signature and (b) K_{DP} core size near the environmental melting layer and 0.5° radial velocity within a downburst's near-surface divergent signature for all downbursts with at least 4 volume scans of data (n = 75). Data used include "traditional-update" data from the operational WSR-88D network and rapid-update KOUN data degraded (i.e., retained every third volume scan) to closely match the volumetric update time of the WSR-88D network. Red markers indicate statistically significant correlations (90% confidence level).

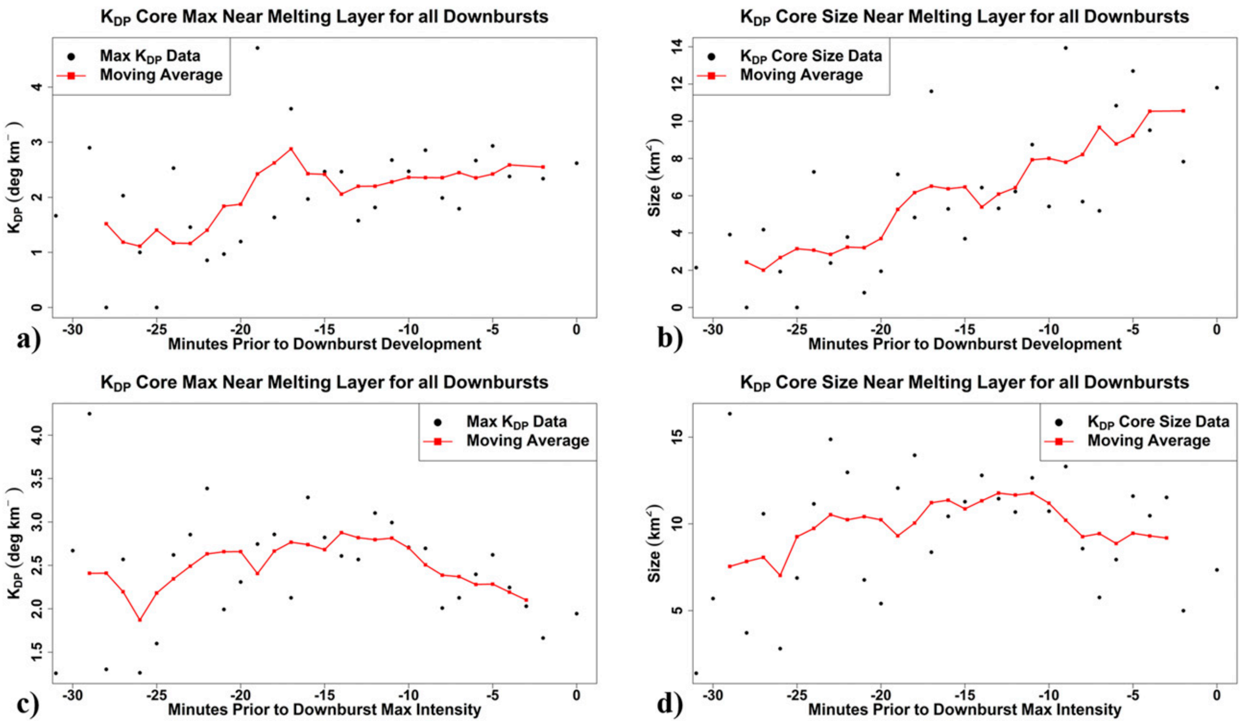

FIG. 2. Average time series for (a) K_{DP} core maximum near the environmental melting layer, (b) K_{DP} core size near the environmental melting layer for the approximately 30-min period prior to *downburst development* as well as (c) K_{DP} core maximum near the environmental melting layer, and (d) K_{DP} core size near the environmental melting layer for the approximately 30-min period prior to *downburst maximum intensity* across all 81 analyzed downbursts. Black dots are the average K_{DP} core data at each available time step, and the red line is the moving average (five time step window that spans ~5 min) of the average K_{DP} core data.

Another clear signal regarding K_{DP} core evolution relative to downburst evolution was observed in time series, averaged across all 81 downbursts, for K_{DP} core maximum and size during the ~30-min period preceding downburst development and maximum intensity. The average time between downburst development and maximum intensity for these downbursts was 10.5 min, so there is some overlap in these 30-min time periods. To produce the time series, we grouped radar observations near the environmental melting layer into time steps (rounded to the nearest whole minute) based on the observation's time relative to downburst development or maximum intensity. Then, using moving averages over a five time step window (~5 min; red lines in Fig. 2), we observed a general increasing trend in K_{DP} core maximum beginning about 25 min prior to downburst development. The most rapid increase in K_{DP} core maximum occurs between 25 and 17 min prior to downburst development and then decreases for a few minutes, but K_{DP} core maximum increases up to the time of downburst development in general (Fig. 2a). This increasing trend is especially clear in K_{DP} core size evolution, where K_{DP} core size nearly continuously increases beginning about 30 min prior to downburst development (Fig. 2b). We also observed an absolute peak in K_{DP} core maximum and size about 14 and 11 min prior to downburst maximum intensity, respectively (Figs. 2c,d).

Based on this analysis, the development and subsequent increase in K_{DP} core maximum or size near the environmental melting level could alert a forecaster that a downburst will develop in the next 30 min. Similarly, a peak and subsequent decreasing trend in K_{DP} core maximum or size could alert a forecaster that the downburst will peak in intensity in the next ~10–15 min. These trends may be difficult to identify in real time especially if they are subtle and/or if there are numerous storms requiring analysis, so creating an algorithm designed to monitor trends in K_{DP} for individual storms may be an important future activity based on our findings. However, even without trend information, determined by an algorithm or not, simply observing a K_{DP} core near the environmental melting layer should increase confidence that a downburst will develop soon. Since our study only considered wet downbursts (section 2), we cannot say that dry downbursts would also be associated with K_{DP} cores near the environmental melting layer, but after looking at a case in Colorado that had three dry downbursts without K_{DP} cores, we expect that this signature may be exclusive to wet downbursts common in the Southern Great Plains and Southeast.

b. Strong and weak downbursts

After observing that K_{DP} cores near the environmental melting layer precede downburst development, we next examined if K_{DP} core characteristics differed between downbursts of different intensities. While there were statistically significant differences between strong and weak downbursts in terms of K_{DP} core maximum and size, there was also overlap between the distributions (Fig. 3). For example, a K_{DP} core maximum of 3° km^{-1} or a K_{DP} core size of 5 km^2 falls within the interquartile range of the distributions for strong and weak downbursts. These values may indicate a greater possibility of a strong downburst, since the values are closer to the median of strong downbursts than weak downbursts and higher values are more commonly associated with strong than weak downbursts in this dataset, but this overlap between the distributions could limit a forecaster's ability to determine if an impending downburst is likely to be strong or weak. This limitation could make it challenging to communicate potential impacts and/or issue warnings regarding an impending downburst.

Despite the similarities between the K_{DP} cores of strong and weak downbursts, there were significant differences between the K_{DP} cores of the two null events (i.e., K_{DP} cores with no downbursts) and the 81 downburst-producing events. The two null events had much lower K_{DP} core maximums and smaller sizes than the weak and strong downbursts (not shown) and only one volume scan had K_{DP} greater than 1.0° km^{-1} near the environmental melting layer. Even though K_{DP} cores near the environmental melting layer may not be able to provide definitive information about how strong an impending downburst might be, they do appear to provide reliable information about whether or not a downburst will develop within a useful amount of time, at least based on this dataset.

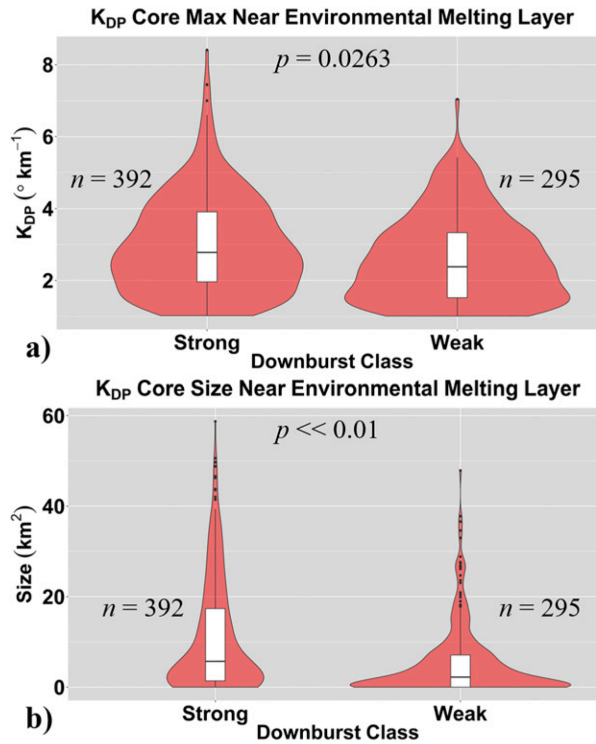

FIG. 3. Violin plots showing the distribution of (a) K_{DP} core maximum and (b) K_{DP} core size at the elevation angle closest to the environmental melting layer for all strong ($n = 50$) and weak ($n = 31$) downbursts. The red area shows the probability density with a greater width indicating a higher frequency of occurrence. Associated box plots are included within each violin plot for reference. Box edges are the lower (Q1) and upper (Q3) quartiles, the horizontal black line is the median, and outliers are indicated by black dots. K–S test p values and number of volume scans (n) used to create each violin plot are also included.

5. Vertical gradient of K_{DP} in K_{DP} cores

Since K_{DP} core characteristics near the environmental melting layer did not provide an overly clear signal about an impending downburst's intensity and numerical simulations have suggested a relationship between the vertical gradient of K_{DP} within a downdraft and the cooling rate (e.g., Ryzhkov et al. 2013; Carlin and Ryzhkov 2019), we examined the vertical gradient of K_{DP} within the K_{DP} cores of all 81 downbursts. To quantify vertical gradient over three different depths, we calculated the difference between K_{DP} maximum, median, and size within the ≥1.0° km^{-1} core between the first elevation angle above the environmental melting layer to the elevation angle closest to either 1, 2, or 3 km below the environmental melting layer. These vertical gradient values were then multiplied by −1 so that any instance of K_{DP} core median, maximum, or size increasing with decreasing height would be a positive value while any instance of K_{DP} core median, maximum, or size decreasing with decreasing height would be a negative value. We performed calculations in this way so that a positive vertical gradient would indicate a potential increase in downdraft intensity as it descended toward the surface.

a. Determining the most reliable measures of K_{DP} core vertical gradients

We looked at several ways of quantifying K_{DP} core vertical gradients including three different depths, described above, and the K_{DP} core metric (i.e., median, maximum, or size) used. There are also different time periods to consider and assumptions that can be made about the data. We calculated statistical significance using Kolmogorov–Smirnov (K–S) tests to explore which combination of variables and assumptions might provide the most consistent and useful measure to forecasters who may want to examine vertical gradients within K_{DP} cores to anticipate downburst intensity.

From the calculated K–S test p values, the K_{DP} core metric associated with the most statistically significant differences between strong and weak downbursts was K_{DP} core size over a depth of about 2 km. Based on this dataset, it is possible that the most effective way for a forecaster to use K_{DP} core gradient for anticipating downburst intensity would be to look at changes in K_{DP} core size between the environmental melting layer and 2 km below it, though an algorithm may be needed to most effectively represent this change. We suspect K_{DP} core size may be related to downdraft cooling because larger cores typically have greater maximum K_{DP} values (not shown) and could also indicate a larger area of melting as well as greater quantities of melting hydrometeors.

We also tested two assumptions regarding the data. Theoretically, we expect that K_{DP} at and above the melting layer would be near 0° km^{-1} within a downdraft primarily composed of dry hail, graupel, and snow. K_{DP} would then increase as the hail, graupel, and snow melted while descending below the environmental melting layer. However, we did not often observe K_{DP} of ~$0°\,km^{-1}$ near the environmental melting layer, perhaps because the downdrafts in our cases are composed of a mixture of wet and dry hail and graupel, raindrops, and snow just above the melting layer, which would result in positive K_{DP}. It is also possible that the K_{DP} column of a weakening updraft would overlap with the K_{DP} core of a developing downdraft, which could cause positive K_{DP} near the melting layer, especially in low-shear environments. Nevertheless, since K_{DP} just above the melting layer would theoretically be near $0°\,km^{-1}$, we set K_{DP} at the elevation angle just above the environmental melting layer (typically within 400 m of the environmental melting layer's approximate height) to $0°\,km^{-1}$ and then calculated vertical gradient as normal. Our other assumption is related to when the K_{DP} core was likely to be at its most intense/mature. Assuming the first and last 25% of volume scans in a K_{DP} core's life cycle represent the most likely development and dissipation times, we limited our vertical gradient calculations to only the middle 50% of volume scans of a K_{DP} core's life cycle, which ranged from about 5 to 35 min.

These assumptions also made a difference when we compared the K–S tests for all K_{DP} core metrics. The method of assuming K_{DP} was $0°\,km^{-1}$ near the environmental melting layer was associated with the most statistically significant differences between strong and weak downbursts. Simply considering all volume scans with no assumptions was associated with the next most statistically significant differences, followed by the method of only considering the middle 50% of volume scans (i.e., mature K_{DP} cores). Therefore, it is possible that assuming K_{DP} just above the environmental melting layer is $0°\,km^{-1}$ may help forecasters use K_{DP} core vertical gradient to anticipate downburst intensity. These assumptions would be difficult for forecasters to apply in real-time operations but could be used as a basis to develop a detection algorithm.

b. Strong and weak downbursts

Regardless of the metrics or assumptions mentioned above, statistically significant differences between strong and weak downbursts were observed with all methods, but similar to K_{DP} core characteristics near the environmental melting layer, there was a lot of overlap between the distributions (Fig. 4). For example, when looking at the vertical gradient of quasi-horizontal K_{DP} core size over a depth of about 2 km, assuming a K_{DP} of $0°\,km^{-1}$ near the environmental melting layer provided the largest statistical significance and the least overlap in the distributions between strong and weak downbursts (Fig. 4a). Despite these differences being larger than comparing all volume scans without assumptions (Fig. 4b) and only considering the middle 50% of volume scans (Fig. 4c), the resulting overlap may make it difficult to use K_{DP} core vertical gradients to anticipate downburst intensity in real-time operations. To illustrate this idea, consider a vertical K_{DP} core size gradient of $8.25\,km^2\,km^{-1}$ (i.e., the size increases by $8.25\,km^2$ per vertical kilometer), representing the median gradient of all strong downbursts (Fig. 4a). This value also lies within the interquartile range of gradients associated with weak downbursts. Larger gradients are more typically associated with strong downbursts, but since this association is not always the case, using a threshold of K_{DP} core size gradient alone to make a warning decision is likely not advisable. This overlap is also greater when not assuming K_{DP} is $0°\,km^{-1}$ near the environmental melting layer (Figs. 4b,c) and for the maximum and median values of K_{DP} core vertical gradients (not shown). However, for all metrics and

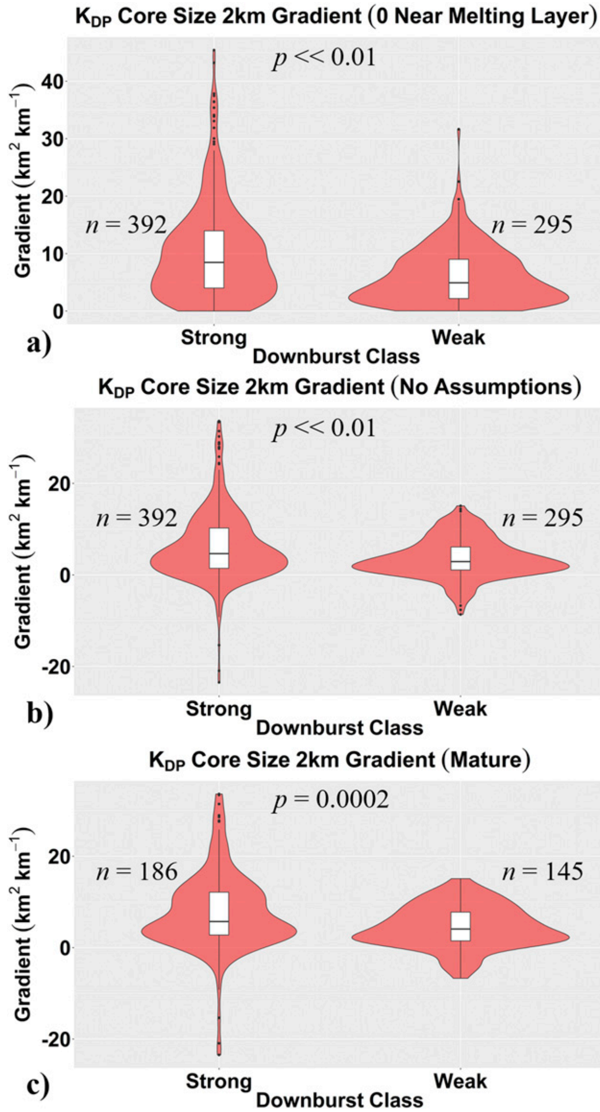

FIG. 4. Violin plots of the vertical gradient of K_{DP} core size over a depth of about 2 km for (a) assuming K_{DP} is $0°\,km^{-1}$ at the elevation angle just above the environmental melting layer, (b) using all volume scans with no assumptions, and (c) only considering the middle 50% of volume scans for each K_{DP} core for all strong (n = 50) and weak (n = 31) downbursts. The red area shows the probability density with a greater width indicating a higher frequency of occurrence. Associated box plots are included within each violin plot for reference. Box edges are the lower (Q1) and upper (Q3) quartiles, the horizontal black line is the median, and outliers are indicated by black dots. K–S test p values and number of volume scans (n) used to create each violin plot are also included.

assumptions, greater vertical gradients could give forecasters more confidence in the likelihood of a downburst being strong and potentially impactful to life and property, especially when considered in the context of conceptual models (section 3) and environmental conditions (section 6).

c. Vertical profile of K_{DP}

Visualizing how K_{DP} core characteristics change with height may be important for understanding and applying information about K_{DP} core vertical gradients (section 5b) in downburst conceptual models and warning decisions. To examine the K_{DP} core vertical profile across all downbursts in our dataset, we calculated mean K_{DP} core maximum, median, and size at all available heights relative to the environmental melting layer (Fig. 5). In general, as one moves downward toward the ground from high altitudes, K_{DP} core maximum, median, and size rapidly increase within about 0.25 km of the approximate height of the environmental melting layer likely in response to the onset of melting of small hail and graupel. These increases are likely accompanied by significant cooling and intensification of the downdraft (section 3). After these increases, K_{DP} core maximum, median, and size level off or decrease over a depth of about 1 km.

The K_{DP} core maximum, median, and size then increase rapidly again until a height of about 2.25–2.5 km below the environmental melting layer. K_{DP} core maximum and median then decrease very slightly (Figs. 5a,b) while K_{DP} core size decreases by about 2 km^2 on average (Fig. 5c). The reverse in sign of the vertical gradients of K_{DP} core maximum, median, and size may signify that 1) evaporation of raindrops has become the dominant microphysical process, which still causes cooling within the downdraft, 2) drop breakup and meltwater shedding is occurring, which do not cause any cooling within the downdraft, and 3) a lack of water-coated hail due to complete melting of the hailstones. This sign reversal may also account for some of the reason why we did not observe strong differences between the vertical gradients of strong and weak downbursts presented in section 5b. For a significant depth (i.e., ~2–2.5 km) below the environmental melting layer, a positive gradient of K_{DP} core maximum or median would be favorable for downdraft strengthening since it is indicative of melting. Below that height, it is possible that a negative gradient would be favorable for downdraft strengthening since it is indicative of evaporation. In our discussion in section 5b, we only looked at positive gradients as favorable for downdraft intensification since our focus was on K_{DP} core intensification, which is indicative of melting hydrometeors. Future work could examine various heights relative to the environmental melting layer for both positive and negative vertical gradients and what they may mean for anticipating downburst intensity.

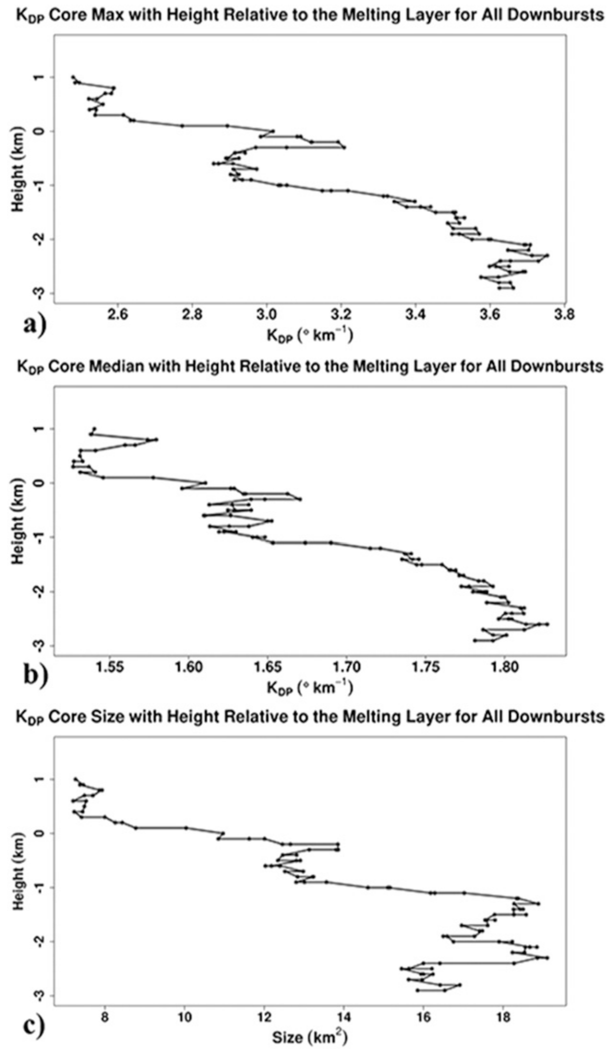

FIG. 5. Vertical profiles of average (a) K_{DP} core maximum, (b) K_{DP} core median, and (c) K_{DP} core size relative to the approximate height of the environmental melting layer across all 81 analyzed downbursts. The 0 on the y axis marks the approximate height of the environmental melting layer.

6. K_{DP} cores and environmental conditions

To examine the near-storm environment, we chose one centrally located (in time and space) latitude–longitude point that would represent the approximate near-storm environment of all downbursts occurring on a given day. We chose this straightforward approach based on the temporal and spatial resolution of the environmental data and due to ambient environmental conditions being relatively stable over the typical duration of a downburst event. Archived mesoanalysis data (grid spacing of 40 km) from the Storm Prediction Center were then used to determine various environmental conditions and parameters (Table 2). To compare environmental variables with K_{DP} core characteristics, we applied the single daily value for each environmental parameter to each volume scan associated with downbursts occurring on that day.

a. K_{DP} core characteristics in favorable and less favorable environments

We did not observe any strong relationships between environmental variables and downburst intensity in our dataset,

TABLE 2. Environmental indicators used, their median values used to define more and less favorable environments for downburst development, p value associated with the differences in K_{DP} core maximum near the environmental melting layer between more and less favorable conditions for downburst development, and parameter values during a case example on 9 Jun 2018. An asterisk (*) indicates that more favorable environmental parameter values were associated with stronger K_{DP} cores rather than more favorable environmental parameter values being associated with weaker K_{DP} cores.

Environmental parameter	Median value	p value for more and less favorable environments relative to max K_{DP} near the environmental melting layer	Environmental parameter value on 9 Jun 2018
DCAPE	1100 J kg^{-1}	0.0003	780.5 J kg^{-1}
Low-level (0–3 km) lapse rate	8°C km^{-1}	0.0196	7.46°C km^{-1}
Low-level (0–3 km) θ_e difference	20 K	0.0043*	19.62 K
Microburst composite parameter	4	0.1178	2
Mixed-layer CAPE	1965 J kg^{-1}	0.0007*	1098.5 J kg^{-1}
Freezing level	4500 m	0.0150	4041 m
Surface dewpoint depression	11.3°C	$\ll$0.01	7.72°C

but we did observe one interesting pattern regarding environmental variables with respect to K_{DP} core characteristics. Larger values of K_{DP} at the elevation angle closest to the environmental melting layer were typically associated with downbursts occurring in environments that previous modeling and observational studies (e.g., Srivastava 1985; Proctor 1989; Atkins and Wakimoto 1991) have suggested are less favorable for downbursts [e.g., lower downdraft convective available potential energy (DCAPE); Fig. 6 and Table 2]. Only two parameters—100-hPa mixed-layer convective available potential energy (MLCAPE) and low-level (0–3 km) θ_e difference—showed the opposite of this pattern (i.e., larger values of K_{DP} in a more favorable environment) Additionally, we binned environmental conditions based on their median values across our 24 case days and then compared the K_{DP} core characteristics of strong and weak downbursts within more and less favorable environments for downburst development (i.e., top and bottom 50%, respectively). From this

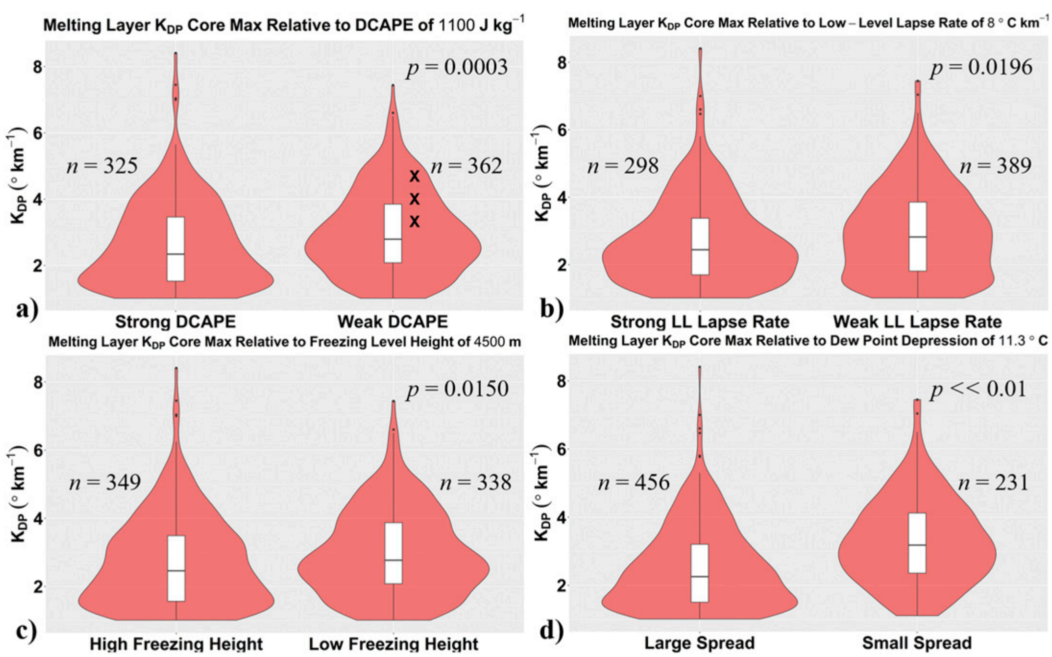

FIG. 6. Violin plots of K_{DP} core maximum near the environmental melting layer relative to the median value of (a) downdraft convective available potential energy (DCAPE), (b) low-level (0–3 km) lapse rates, (c) freezing level height, and (d) dewpoint depression. The X marks in (a) indicate the median K_{DP} core maximums of the three downbursts that occurred on 9 Jun 2018. The red area shows the probability density with a greater width indicating a higher frequency of occurrence. Associated box plots are included within each violin plot for reference. Box edges are the lower (Q1) and upper (Q3) quartiles, the horizontal black line is the median, and outliers are indicated by black dots. K–S test p values and number of volume scans (n) used to create each violin plot are also included.

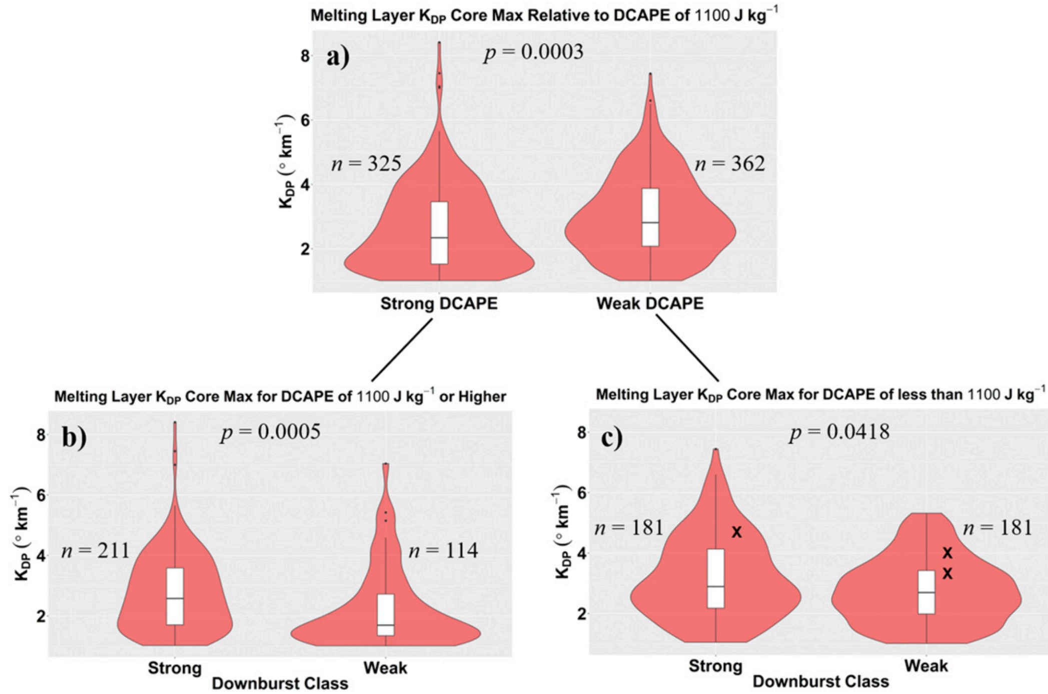

FIG. 7. Violin plots showing K_{DP} core maximum near the environmental melting layer using a median DCAPE value of 1100 J kg^{-1} to illustrate differences between (a) more and less favorable environments for downburst development, (b) strong and weak downbursts in a more favorable environment, and (c) strong and weak downbursts in a less favorable environment. The X marks in (c) indicate the median K_{DP} core maximums of the three downbursts that occurred on 9 Jun 2018. The red area shows the probability density with a greater width indicating a higher frequency of occurrence. Associated box plots are included within each violin plot for reference. Box edges are the lower (Q1) and upper (Q3) quartiles, the horizontal black line is the median, and outliers are indicated by black dots. K–S test p values and number of volume scans (n) used to create each violin plot are also included.

comparison, we found that strong downbursts typically had higher values of K_{DP} near the environmental melting layer than weak downbursts, especially when using DCAPE or surface dewpoint depression to classify the environment (Figs. 6 and 7).

These observations make sense because as the environment becomes less favorable for downbursts, more melting, evaporation, and precipitation loading may be needed for a downburst to develop. The simulation results of Srivastava (1987) also indicated a similar pattern where greater precipitation mixing ratios, rainfall rates, and radar reflectivities were needed for robust downburst development as the low-level temperature lapse rate decreased (i.e., environment became less favorable for downbursts). The corroboration of simulation-based results of Srivastava (1987) and our radar-based results could be helpful to forecasters with a knowledge of environmental conditions who are making warning decisions regarding downbursts. If the ambient environment is less favorable for downburst development—smaller DCAPE for example—then a higher K_{DP} core maximum near the environmental melting layer would be needed to anticipate a strong downdraft (Figs. 6 and 7). Conversely, if the environment is more favorable for downbursts, a lower warning threshold of K_{DP} core maximum near the environmental melting layer could be considered. The development of hard warning thresholds using K_{DP} cores alone is not ideal, but K_{DP} cores near the environmental melting layer could aid forecasters in a qualitative assessment of downburst risk, which would add information to the downburst conceptual model and could allow for a triage of multiple storms in a similar environment to determine which ones may pose the greatest downburst risk.

b. A case example

On 9 June 2018, a marginal downburst event occurred near Birmingham, Alabama. The closest WSR-88D (KBMX) was operated using volume coverage pattern 215 and had a volumetric update time of about 5.8 min. From this data we identified three downbursts for analysis. One produced tree and power line damage and was classified as strong, while the other two were not associated with a wind report or radial velocities ≥ 23 m s^{-1} and were classified as weak. The environment was characterized by very weak shear and steep low-level lapse rates (Fig. 8). Since all environmental parameters, except low-level θ_e difference, were below the 25th percentile of parameters across all analyzed cases

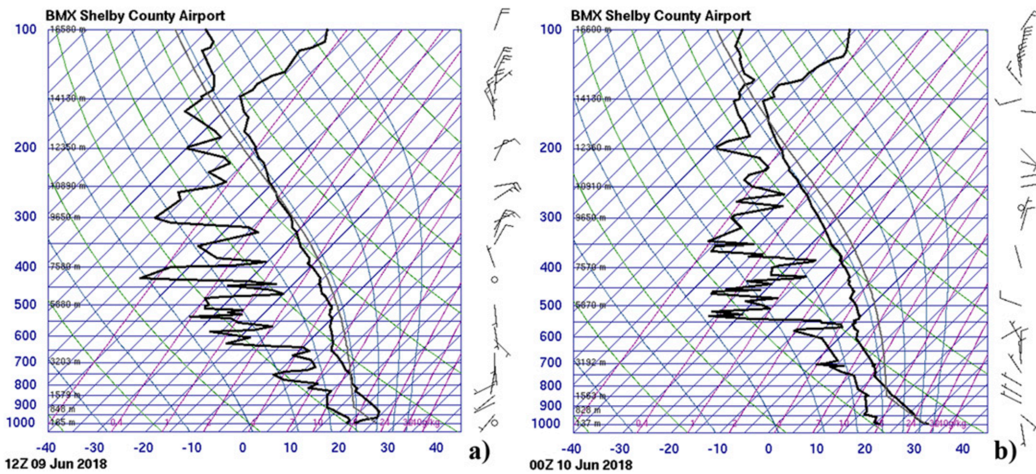

FIG. 8. Observed soundings at (a) 1200 UTC 9 Jun 2018 and (b) 0000 UTC 10 Jun 2018 taken from just south of Birmingham, AL (BMX; Shelby County Airport) and relatively close (~30 km) to the analyzed downbursts' location. Sounding images and data are available through the University of Wyoming (http://weather.uwyo.edu/upperair/sounding.html).

(Table 2), we considered this a less favorable environment for downbursts.

With a less favorable environment, it is not surprising that the downburst-producing storms had relatively high K_{DP} core maximums near the environmental melting layer. Median K_{DP} core maximums for all three downbursts were above the median for all downbursts occurring in a less favorable environment and two out of the three were above the 75th percentile (Figs. 6a and 7c). A clear K_{DP} core near the environmental melting layer was also present prior to the 0.5° divergent signature of all three downbursts and prior to the wind report associated with the strong downburst.

For the strong downburst, a K_{DP} core first developed near and below the environmental melting layer at 0015:29 UTC or about 11.5 min prior to initial downburst development and 31.5 min prior to the first wind report associated with this slowly evolving downburst (Figs. 9a, 10a, and the supplemental material). The K_{DP} core generally intensified (i.e., maximum values increased) over the next several volume scans and reached peak intensity (i.e., highest K_{DP} values) at 0033:02 (Figs. 9b–d). During this time, the K_{DP} core also elongated in the vertical and reached the lowest-elevation angle at about 0027:06 UTC, which was also about the same time the 0.5° divergent signature developed (Figs. 9c and 10a–c). After 0033:02, the K_{DP} core near the environmental melting layer then generally weakened and shrank in areal extent through the time of the wind report and downburst maximum intensity at 0047 and 0050 UTC, respectively (Figs. 9e–h). In the vertical, despite maximum values of K_{DP} generally decreasing, a nearly continuous area of $\geq 1°\ km^{-1}$ extended from near the surface to near the environmental melting layer through the time of downburst maximum intensity around 0050:30 UTC (Figs. 10e–g). During this time, the K_{DP} core size gradient over a depth of about 2 km ranged from about 4.6 to 7.0 $km^2\ km^{-1}$, which was near or slightly above the median for all strong downbursts (Figs. 4b and 10e–g). The K_{DP} core then continued to weaken after this time (Figs. 9h and 10h) and dissipated just after 0100 UTC (not shown).

7. Rapid-update observations of K_{DP} cores

We examined the potential impact of volumetric radar update time in observing K_{DP} cores by comparing results using rapid-update (i.e., volumetric update times of 1.8–2.2 min) data provided by KOUN and ''traditional-update'' (i.e., volumetric update times of 4.0–7.1 min) data provided by the operational WSR-88D network. Surprisingly, we observed few differences between the rapid-update and traditional-update data in terms of K_{DP} core characteristics between strong and weak downbursts. Statistical significance did not change much regardless of the volumetric update time used. However, we only had a relatively small sample size (16 downbursts and 219 volume scans) of rapid-update KOUN data available, so that may have impacted these results.

One potential explanation for our observation is that K_{DP} cores evolve relatively slowly, typically taking 15–35 min to develop and intensify to peak magnitude. This slower evolution, compared to other known downburst precursor signatures, may occur because melting can persist near the environmental melting layer as long as there is modest convection that can generate hail/graupel that would melt as it falls through the downdraft. Therefore, a K_{DP} core could be present near and below the environmental melting layer even after the leading (i.e., lower) edge of the downdraft has descended toward the surface and/or as multiple downdraft ''pulses'' occur, but more research is needed to confirm this idea. The persistent nature of the K_{DP} core near and below the environmental melting layer observed here potentially makes this an ideal downburst precursor signature to use because operational WSR-88Ds can sample the K_{DP} core

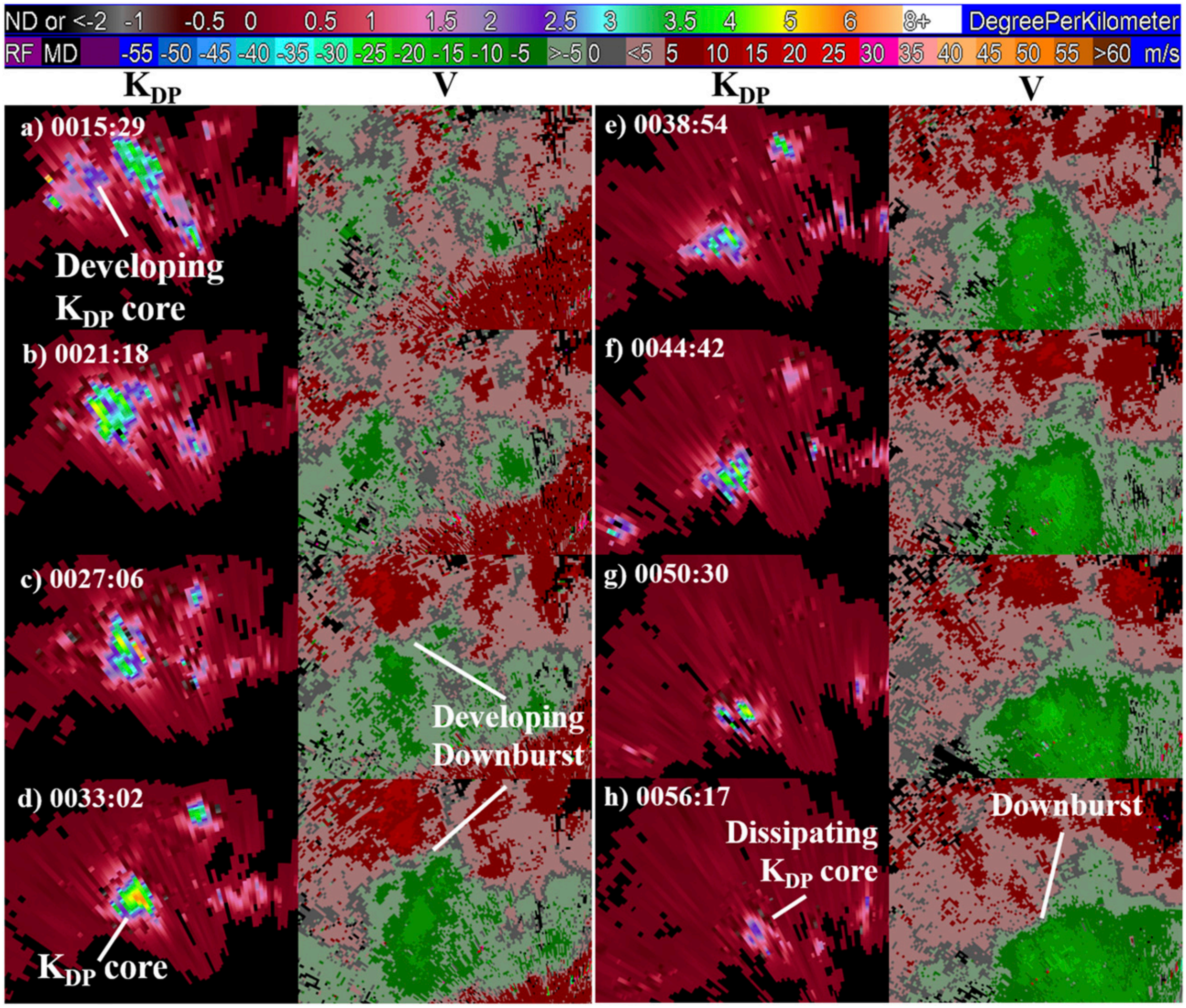

FIG. 9. (left) The K_{DP} at the elevation angle closest to the environmental melting layer (6.4°–10°; 3.5–4.3 km above ground level) and (right) base velocity at the 0.5° elevation angle (0.2–0.4 km above ground level) between (a) 0015:29 and (h) 0056:17 UTC 10 Jun 2018. The K_{DP} core range from radar varies from about 35 km in (a) to 23 km in (h). Color bars for K_{DP} (° km^{-1}) and radial velocity (m s^{-1}) are included at the top. Storm report (several trees uprooted) occurs closest in time to (f) and maximum downburst intensity (maximum radial velocity of 23.5 m s^{-1}) closest to (g).

several times and roughly capture its evolution (Figs. 2, 9, and 10) even at volumetric update times of ~5–6 min. It is also likely easier to observe a K_{DP} core near the environmental melting layer with the WSR-88D network than the descent of a K_{DP} core, which could occur more quickly—similarly to descending reflectivity cores that can descend in 10.5 min or less (e.g., Heinselman et al. 2008; Kuster et al. 2016). It remains possible that faster volumetric update times can capture the short-term evolution of K_{DP} cores and downbursts more effectively than the volumetric update times of the operational WSR-88D network (Fig. 11a) especially when the K_{DP} core evolves more quickly than in most of the cases we examined (e.g., less than 15 min; Fig. 11b). Rapid-update volumetric data would also likely be beneficial in sampling other quickly evolving downburst precursor signatures and in sampling additional characteristics of K_{DP} cores, such as their descent.

8. Summary

Downbursts, especially those associated with short-lived "pulse" thunderstorms in low-shear environments, can pose a forecast and warning challenge to operational meteorologists. The goal of this study is to present information about a little-known and little-used dual-pol downburst precursor signature, known as a K_{DP} core, that could help forecasters anticipate downburst development and potential intensity. Through an analysis of 81 downbursts spanning 24 different days across 10 states (Table 1), we conclude the following:

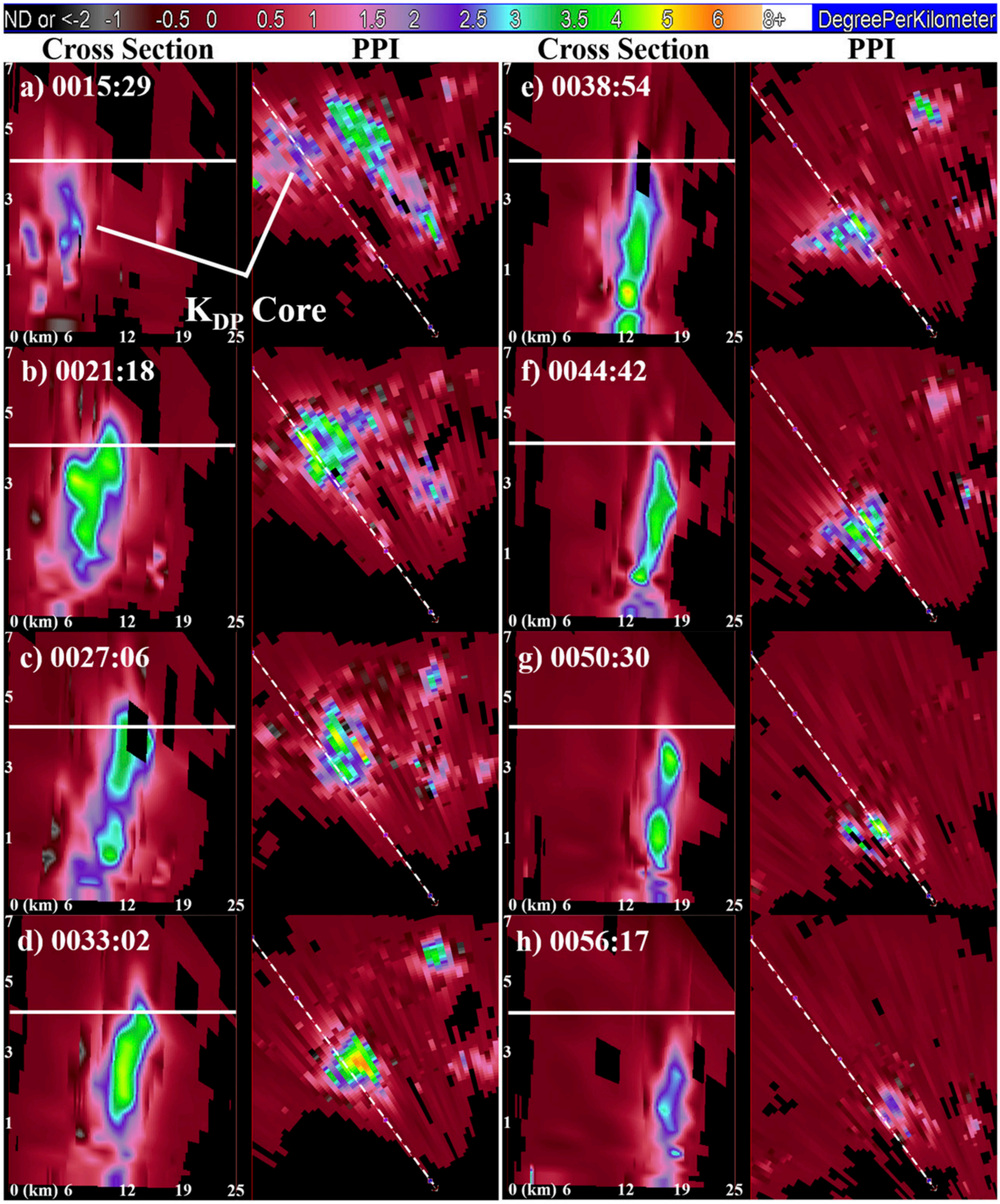

FIG. 10. (left) Vertical cross sections and (right) planned position indicators (PPI) of a K_{DP} core between (a) 0015:29 and (h) 0056:17 UTC 10 Jun 2018. The horizontal white line in each panel indicates the approximate height of the environmental melting layer (~4.2 km above mean sea level), while the diagonal dashed white line indicates the location of the vertical cross section. The K_{DP} core range from radar varies from ~35 km in (a) to ~23 km in (i). PPI elevation angle is elevation angle closest to the environmental melting layer (6.4°–10°; 3.5–4.3 km above ground level). The color bar for K_{DP} (° km^{-1}) is included at the top. Storm report (several trees uprooted) occurs closest in time to (f) and maximum downburst intensity (maximum radial velocity of 23.5 m s^{-1}) closest to (g).

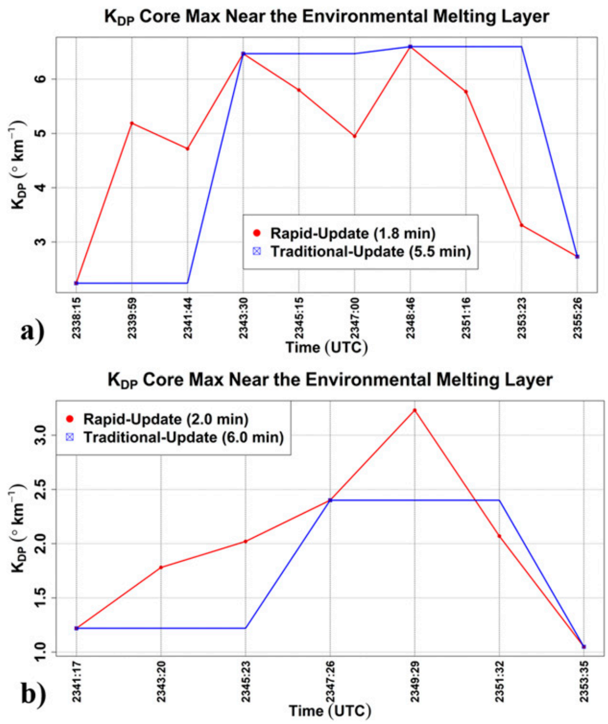

FIG. 11. The K_{DP} core maximum evolution depicted by rapid-update KOUN data (red line) and degraded (i.e., retained every third volume scan) KOUN data that are similar in volumetric update time to the operational WSR-88D network (i.e., "traditional update"; blue line) for a downburst-producing storm on (a) 30 Jun 2016 and (b) 8 Jul 2014 in central Oklahoma.

1) The K_{DP} cores near the environmental melting layer likely precede the development and intensification of downbursts. Every downburst in our study was associated with a K_{DP} core, and we could only identify two K_{DP} cores that were not associated with a downburst.
2) Using K_{DP} cores to anticipate the potential intensity and therefore impacts of an impending downburst may be difficult since overlap exists between the K_{DP} core characteristics associated with strong (i.e., wind report or maximum radial velocity $\geq 23\,\mathrm{m\,s^{-1}}$) and weak downbursts in this dataset. This overlap occurs with K_{DP} core characteristics near the environmental melting layer and with the vertical gradient of K_{DP}.
3) Despite the overlap mentioned above, higher K_{DP} core maximums and larger gradients are more frequently observed with strong downbursts. For strong downbursts in our study, the 50th percentile of K_{DP} core maximum and size near the environmental melting layer was 2.78° km^{-1} and 5.69 km^2, respectively, and the 50th percentile of K_{DP} core size vertical gradient over a depth of about 2 km was 4.64 km^2 km^{-1} (Figs. 3 and 4b).
4) Stronger (i.e., higher maximum values or larger sizes) K_{DP} cores are likely needed for downburst development when environmental conditions are less favorable for downbursts (e.g., smaller low-level lapse rates). The K_{DP} cores can likely help forecasters triage storms to determine which are most likely to produce downbursts across areas with similar environmental conditions.
5) The K_{DP} cores evolve over times typically longer than 15 min. This duration is relatively favorable for observations made using the operational WSR-88D network with volumetric updates times of about 5 min because multiple volume scans will be able to sample the K_{DP} core during its lifetime. However, rapid-update volumetric radar data may still provide advantages due to better sampling of any short-lived changes in K_{DP} cores.

The results of this study fit well with the conceptual model of wet downburst development where precipitation loading and the melting of small graupel and hail contribute to the development and intensification of a downdraft. Integrating K_{DP} cores into this conceptual model will likely provide forecasters with greater understanding of the conceptual model in the context of ongoing storms and improve the ability to anticipate impending downbursts and their potential impacts especially for storms within 100 km of a radar. This anticipation includes not only downbursts with severe winds, but also lesser magnitude events that are still relevant to forecasters especially during event support where venues may have lower wind thresholds for making decisions.

However, there are likely some important limitations to consider. It is likely that K_{DP} cores are very rare in the dry environments typically present across the western United States. We did not observe any K_{DP} cores when looking at a case in Colorado containing three dry downbursts and expect that K_{DP} cores will only be commonly observed in regions with moister environments typically associated with wet downbursts and greater depths with appreciable melting of hail. Even in regions with more saturated environments, melting and precipitation loading are not the only factors that influence downburst development and intensity, so K_{DP} cores alone cannot be used to successfully anticipate downbursts. Quantifying other radar variables (e.g., Z, Z_{DR}) within K_{DP} cores could be beneficial in determining a storm's downburst potential and is a topic of future work. Environmental conditions, other radar signatures, observations, and scientific conceptual models must be used in concert with K_{DP} cores to most effectively anticipate downburst development and intensity.

Despite these limitations, we expect K_{DP} cores can be a reliable downburst precursor signature—in environments supportive of wet downbursts—now and as radar technology and scanning strategies advance and allow for faster volumetric update times and improved spatial resolution. A future dual-pol phased array radar network with better coverage than the existing WSR-88D network could prove useful for downburst detection since it would provide rapid updates near the surface to monitor a downburst's low-level divergent signature as well as rapid updates and super-resolution data at higher-elevation angles to monitor K_{DP} core evolution. Any scanning strategy or data processing technique that decreases volumetric update time or increases spatial resolution of the WSR-88D network may also improve K_{DP} core observations, which could further help forecasters, algorithm developers, researchers using machine learning (e.g., Lagerquist et al. 2017; Medina et al. 2019), and initiatives like Warn-on-Forecast (e.g., Stensrud et al. 2009; Lawson et al. 2018) use K_{DP} cores to anticipate downburst development.

Acknowledgments. CK thanks God for providing the opportunity and talented research team to accomplish this research. Specifically, the authors thank Eddie Forren for KOUN data processing; Danny Wasielewski, Micheal Shattuck, Allen Zahrai, and Rafael Mendoza for KOUN data collection support; and Richard Smith, David Andra, and Todd Lindley of NWS Norman for research support. We also thank Tanya Riley, Tracy Reinke, Jamie Foucher, Mandi Campbell, and Colleen Hickman for help with administrative logistics; and Steve Fletcher, Chris Carter, Jeff Horn, and everyone at NSSL IT for help with computer software/hardware and telework support. We also thank Jeffrey Snyder and Todd Lindley for their helpful internal reviews, and three reviewers who helped improve the quality of this paper. Funding for CK, JC, TS, JB, and RT was provided by NOAA/Office of Oceanic and Atmospheric Research under NOAA–University of Oklahoma Cooperative Agreement NA16OAR4320115, U.S. Department of Commerce.

Data availability statement. KOUN radar data can be requested from the National Severe Storms Laboratory, while WSR-88D data are available at the National Centers for Environmental Information's Radar Archive (https://www.ncdc.noaa.gov/nexradinv/).

REFERENCES

Amiot, C. G., L. D. Carey, W. P. Roeder, T. M. McNamara, and R. J. Blakeslee, 2019: C-band dual-polarization radar signatures of wet downbursts around Cape Canaveral, Florida. *Wea. Forecasting*, **34**, 103–131, https://doi.org/10.1175/WAF-D-18-0081.1.

Atkins, N. T., and R. M. Wakimoto, 1991: Wet microburst activity over the southeastern United States: Implications for forecasting. *Wea. Forecasting*, **6**, 470–482, https://doi.org/10.1175/1520-0434(1991)006<0470:WMAOTS>2.0.CO;2.

Auer, A. H., Jr., 1972: Distribution of graupel and hail with size. *Mon. Wea. Rev.*, **100**, 325–328, https://doi.org/10.1175/1520-0493-100-05-0325.

Augros, C., O. Caumont, V. Ducrocq, N. Gaussiat, and P. Tabary, 2016: Comparisons between S-, C-, and X-band polarimetric radar observations and convective-scale simulations of the HyMeX first special observing period. *Quart. J. Roy. Meteor. Soc.*, **142**, 347–362, https://doi.org/10.1002/qj.2572.

Bringi, V. N., T. A. Seliga, and K. Aydin, 1984: Hail detection with a differential reflectivity radar. *Science*, **225**, 1145–1147, https://doi.org/10.1126/science.225.4667.1145.

Brock, F. V., K. C. Crawford, R. L. Elliot, G. W. Cuperus, S. J. Stadler, H. L. Johnson, and M. D. Eilts, 1995: The Oklahoma Mesonet: A technical overview. *J. Atmos. Oceanic Technol.*, **12**, 5–19, https://doi.org/10.1175/1520-0426(1995)012<0005:TOMATO>2.0.CO;2.

Carlin, J. T., and A. V. Ryzhkov, 2019: Estimation of melting-layer cooling rate from dual-polarization radar: Spectral bin model simulations. *J. Appl. Meteor. Climatol.*, **58**, 1485–1508, https://doi.org/10.1175/JAMC-D-18-0343.1.

——, ——, J. C. Snyder, and A. Khain, 2016: Hydrometeor mixing ratio retrievals for storm-scale radar data assimilation: Utility of current relations and potential benefits of polarimetry. *Mon. Wea. Rev.*, **144**, 2981–3001, https://doi.org/10.1175/MWR-D-15-0423.1.

Field, P. R., A. J. Heymsfield, A. G. Detwiler, and J. M. Wilkinson, 2019: Normalized hail particle size distributions from the T-28 storm-penetrating aircraft. *J. Appl. Meteor. Climatol.*, **58**, 231–245, https://doi.org/10.1175/JAMC-D-18-0118.1.

Forsyth, D. E., and Coauthors, 2005: The National Weather Radar Testbed (phased array). *32nd Conf. on Radar Meteorology*, Albuquerque, NM, Amer. Meteor. Soc., 12R.3, https://ams.confex.com/ams/32Rad11Meso/techprogram/paper_96377.htm.

Frugis, B. J., 2018: Using specific differential phase to predict significant severe thunderstorm wind damage across the northeastern United States. *Twenty Ninth Conf. on Severe Local Storms*, Stowe, VT, Amer. Meteor. Soc, 21, https://ams.confex.com/ams/29SLS/meetingapp.cgi/Paper/348206.

——, 2020: The use of collapsing specific differential phase columns to predict significant severe thunderstorm wind damage across the northeastern United States. Eastern Region Tech. Attachment 2020-04, 16 pp., https://www.weather.gov/media/erh/ta2020-04.pdf.

Fujita, T. T., 1981: Tornadoes and downbursts in the context of generalized planetary scales. *J. Atmos. Sci.*, **38**, 1511–1534, https://doi.org/10.1175/1520-0469(1981)038<1511:TADITC>2.0.CO;2.

——, and H. R. Byers, 1977: Spearhead echo and downburst in the crash of an airliner. *Mon. Wea. Rev.*, **105**, 129–146, https://doi.org/10.1175/1520-0493(1977)105<0129:SEADIT>2.0.CO;2.

——, and R. M. Wakimoto, 1981: Five scales of airflow associated with a series of downbursts on 16 July 1980. *Mon. Wea. Rev.*, **109**, 1438–1456, https://doi.org/10.1175/1520-0493(1981)109<1438:FSOAAW>2.0.CO;2.

Heinselman, P. L., and A. V. Ryzhkov, 2006: Validation of polarimetric hail detection. *Wea. Forecasting*, **21**, 839–850, https://doi.org/10.1175/WAF956.1.

——, D. L. Priegnitz, K. L. Manross, T. M. Smith, and R. W. Adams, 2008: Rapid sampling of severe storms by the National Weather Radar Testbed Phased Array Radar. *Wea. Forecasting*, **23**, 808–824, https://doi.org/10.1175/2008WAF2007071.1.

Hubbert, J. V., V. N. Bringi, and L. D. Carey, 1998: CSU–CHILL polarimetric radar measurements from a severe hail storm in eastern Colorado. *J. Appl. Meteor.*, **37**, 749–775, https://doi.org/10.1175/1520-0450(1998)037<0749:CCPRMF>2.0.CO;2.

Isaminger, M. A., 1988: A preliminary study of precursors to Huntsville microbursts. Lincoln Laboratory Project Rep. ATC-153, 28 pp., https://apps.dtic.mil/sti/pdfs/ADA200914.pdf.

Jung, Y., M. Xue, and M. Tong, 2012: Ensemble Kalman filter analyses of the 29–30 May 2004 Oklahoma tornadic thunderstorm using one- and two-moment bulk microphysics schemes, with verification against polarimetric data. *Mon. Wea. Rev.*, **140**, 1457–1475, https://doi.org/10.1175/MWR-D-11-00032.1.

Kingsmill, D. E., and R. M. Wakimoto, 1990: Kinematic, dynamic, and thermodynamic analysis of a weakly sheared severe thunderstorm over northern Alabama. *Mon. Wea. Rev.*, **119**, 262–297, https://doi.org/10.1175/1520-0493(1991)119<0262:KDATAO>2.0.CO;2.

Kumjian, M. R., 2013: Principles and applications of dual-polarization weather radar. Part I: Description of the polarimetric radar variables. *J. Oper. Meteor.*, **1**, 226–242, https://doi.org/10.15191/nwajom.2013.0119.

——, Y. P. Richardson, T. Meyer, K. A. Kosiba, and J. Wurman, 2018: Resonance scattering effects in wet hail observed with a dual-X-band frequency, dual-polarization Doppler on Wheels radar. *J. Appl. Meteor. Climatol.*, **57**, 2713–2731, https://doi.org/10.1175/JAMC-D-17-0362.1.

——, Z. J. Lebo, and A. M. Ward, 2019: Storms producing large accumulations of small hail. *J. Appl. Meteor. Climatol.*, **58**, 341–364, https://doi.org/10.1175/JAMC-D-18-0073.1.

Kuster, C. M., P. L. Heinselman, and T. J. Schuur, 2016: Rapid-update radar observations of downbursts occurring within an intense multicell thunderstorm on 14 June 2011. *Wea. Forecasting*, **31**, 827–851, https://doi.org/10.1175/WAF-D-15-0081.1.

LaDue, D. S., P. L. Heinselman, and J. F. Newman, 2010: Strengths and limitations of current radar systems for two stakeholder groups in the southern plains. *Bull. Amer. Meteor. Soc.*, **91**, 899–910, https://doi.org/10.1175/2009BAMS2830.1.

Lagerquist, R., A. McGovern, and T. Smith, 2017: Machine learning for real-time prediction of damaging straight-line convective wind. *Wea. Forecasting*, **32**, 2175–2193, https://doi.org/10.1175/WAF-D-17-0038.1.

Lawson, J. R., J. S. Kain, N. Yussouf, D. C. Dowell, D. M. Wheatley, K. H. Knopfmeier, and T. A. Jones, 2018: Advancing from convective-allowing NWP to Warn-on-Forecast: Evidence of progress. *Wea. Forecasting*, **33**, 599–607, https://doi.org/10.1175/WAF-D-17-0145.1.

Loney, M. L., D. S. Zrnić, J. M. Straka, and A. V. Ryzhkov, 2002: Enhanced polarimetric radar signatures above the melting layer in a supercell storm. *J. Appl. Meteor.*, **41**, 1179–1194, https://doi.org/10.1175/1520-0450(2002)041<1179:EPRSAT>2.0.CO;2.

Mahale, V. N., G. Zhang, and M. Xue, 2016: Characterization of the 14 June 2011 Norman, Oklahoma downburst through dual-polarization radar observations and hydrometeor classification. *J. Appl. Meteor. Climatol.*, **55**, 2635–2655, https://doi.org/10.1175/JAMC-D-16-0062.1.

McNulty, R. P., 1991: Downbursts from innocuous clouds: An example. *Wea. Forecasting*, **6**, 148–154, https://doi.org/10.1175/1520-0434(1991)006<0148:DFICAE>2.0.CO;2.

McPherson, R. A., and Coauthors, 2007: Statewide monitoring of the mesoscale environment: A technical update on the Oklahoma Mesonet. *J. Atmos. Oceanic Technol.*, **24**, 301–321, https://doi.org/10.1175/JTECH1976.1.

Medina, B. L., L. D. Carey, C. G. Amiot, R. M. Mecikalski, W. P. Roeder, T. M. McNamara, and R. J. Blakeslee, 2019: A random forest method to forecast downbursts based on dual-polarization radar signatures. *Remote Sens.*, **11**, 826, https://doi.org/10.3390/rs11070826.

Miller, P. W., and T. L. Mote, 2018: Characterizing severe weather potential in synoptically weakly forced thunderstorm environments. *Nat. Hazards Earth Syst. Sci.*, **18**, 1261–1277, https://doi.org/10.5194/nhess-18-1261-2018.

Proctor, F. H., 1988: Numerical simulations of an isolated microburst. Part I: Dynamics and structure. *J. Atmos. Sci.*, **45**, 3137–3160, https://doi.org/10.1175/1520-0469(1988)045<3137:NSOAIM>2.0.CO;2.

——, 1989: Numerical simulations of an isolated microburst. Part II: Sensitivity experiments. *J. Atmos. Sci.*, **46**, 2143–2165, https://doi.org/10.1175/1520-0469(1989)046<2143:NSOAIM>2.0.CO;2.

Rasmussen, R. M., and A. J. Heymsfield, 1987: Melting and shedding of graupel and hail. Part I: Model physics. *J. Atmos. Sci.*, **44**, 2754–2763, https://doi.org/10.1175/1520-0469(1987)044<2754:MASOGA>2.0.CO;2.

Roberts, R. D., and J. W. Wilson, 1989: A proposed microburst nowcasting procedure using single-Doppler radar. *J. Appl. Meteor.*, **28**, 285–303, https://doi.org/10.1175/1520-0450(1989)028<0285:APMNPU>2.0.CO;2.

Ryzhkov, A. V., S. E. Giangrande, V. M. Melnikov, and T. J. Schuur, 2005: Calibration issues of dual-polarization radar measurements. *J. Atmos. Oceanic Technol.*, **22**, 1138–1155, https://doi.org/10.1175/JTECH1772.1.

——, M. R. Kumjian, S. M. Ganson, and A. P. Khain, 2013: Polarimetric radar characteristics of melting hail. Part I: Theoretical simulations using spectral microphysical modeling. *J. Appl. Meteor. Climatol.*, **52**, 2849–2870, https://doi.org/10.1175/JAMC-D-13-073.1.

Scharfenberg, K. A., 2003: Polarimetric radar signatures in microburst-producing thunderstorms. *31st Int. Conf. on Radar Meteorology*, Seattle, WA, Amer. Meteor. Soc., 8B.4, https://ams.confex.com/ams/pdfpapers/64413.pdf.

Seliga, T. A., and V. N. Bringi, 1978: Differential reflectivity and differential phase shift: Applications in radar meteorology. *Radio Sci.*, **13**, 271–275, https://doi.org/10.1029/RS013i002p00271.

Smith, T. M., K. L. Elmore, and S. A. Dulin, 2004: A damaging downburst prediction and detection algorithm for the WSR-88D. *Wea. Forecasting*, **19**, 240–250, https://doi.org/10.1175/1520-0434(2004)019<0240:ADDPAD>2.0.CO;2.

Snyder, J. C., H. B. Bluestein, D. T. Dawson II, and Y. Jung, 2017: Simulations of polarimetric, X-band radar signatures in supercells. Part II: Z_{DR} columns and rings and K_{DP} columns. *J. Appl. Meteor. Climatol.*, **56**, 2001–2026, https://doi.org/10.1175/JAMC-D-16-0139.1.

Srivastava, R. C., 1985: A simple model of evaporatively driven downdraft: Application to microburst downdraft. *J. Atmos. Sci.*, **42**, 1004–1023, https://doi.org/10.1175/1520-0469(1985)042<1004:ASMOED>2.0.CO;2.

——, 1987: A model of intense downdrafts driven by the melting and evaporation of precipitation. *J. Atmos. Sci.*, **44**, 1752–1774, https://doi.org/10.1175/1520-0469(1987)044<1752:AMOIDD>2.0.CO;2.

Stensrud, D. J., and Coauthors, 2009: Convective-scale warn-on-forecast system: A vision for 2020. *Bull. Amer. Meteor. Soc.*, **90**, 1487–1500, https://doi.org/10.1175/2009BAMS2795.1.

Straka, J. M., and J. R. Anderson, 1993: Numerical simulations of microburst-producing storms: Some results from storms observed during COHMEX. *J. Atmos. Sci.*, **50**, 1329–1348, https://doi.org/10.1175/1520-0469(1993)050<1329:NSOMPS>2.0.CO;2.

Trapp, R. J., D. M. Wheatley, N. T. Atkins, R. W. Przybylinski, and R. Wolf, 2006: Buyer beware: Some words of caution on the use of severe wind reports in postevent assessment and research. *Wea. Forecasting*, **21**, 408–415, https://doi.org/10.1175/WAF925.1.

Wakimoto, R. M., 1985: Forecasting dry microburst activity over the high plains. *Mon. Wea. Rev.*, **113**, 1131–1143, https://doi.org/10.1175/1520-0493(1985)113<1131:FDMAOT>2.0.CO;2.

——, and V. N. Bringi, 1988: Dual-Polarization observations of microbursts associated with intense convection: The 20 July storm during the MIST project. *Mon. Wea. Rev.*, **116**, 1521–1539, https://doi.org/10.1175/1520-0493(1988)116<1521:DPOOMA>2.0.CO;2.

Wilson, J. W., R. D. Roberts, C. Kessinger, and J. McCarthy, 1984: Microburst wind structure and evaluation of Doppler radar for airport wind shear detection. *J. Climate Appl. Meteor.*, **23**, 898–915, https://doi.org/10.1175/1520-0450(1984)023<0898:MWSAEO>2.0.CO;2.

Zrnić, D. S., and Coauthors, 2007: Agile-beam phased array radar for weather observations. *Bull. Amer. Meteor. Soc.*, **88**, 1753–1766, https://doi.org/10.1175/BAMS-88-11-1753.